Hover Controller Design and Implementation for a Dragonfly-like Flapping Wing

A. Mohammad Lashgari, B. Abolghasem Naghash*
Amirkabir University of Technology , Tehran

Abstract

The aim of this paper is modelling, simulating and designing a controller for a micro aerial vehicle (MAV) as well as implementing an innovative scheme for it. The MAV scheme inspired by the dragonfly using clap and fling mechanism with an active rigid abdomen. The gearboxes are responsible for moving two pairs of four flying wings in front and back of the MAV. Also, change in the motors speed generates differential thrust to create a control pitch moment. The linearization about a hover point is performed to analyze the motion and design an LQR controller. Moreover, validity of the linearized equations is verified by comparing the responses of linear and nonlinear models. The theoretical results are experimented with a hardware-in-the-loop testbed. The experimental results demonstrate good agreement between theoretical and validated responses along with accurate and robust hovering at the desired point.
Keywords: Flapping wing MAV, Active rigid abdomen, Hover controller design, LQR controller.

1 Introduction

Wonderful flights of insects and birds have been noticed by many researchers. Each category of birds and insects has special mechanism for guiding, controlling and producing lift and thrust. Among all flight maneuvers of insects and birds hovering in stationary point [1] with high stability is the determining factor for quality of flight. Hover is the unstable mode of flight and for a flapping wing MAV's is very important [2, 3, 4, 5]. The main concern in this paper is to control the pitch angle for maneuvering in hover for a dragonfly-like, MAV having clap and fling mechanism. Hereafter, we call it as our MAV for short.
There is a valuable work for modeling the nonlinear aerodynamics of a flapping wing in[6] . Precise relationships to calculate lift and drag theoretically and experimentally are introduced in [1] that are used in Section 4.

*Email address:Naghash@aut.ac.ir

To review the role of an active rigid abdomen in a flapping wing MAV there has not been much theoretical or modeling or simulation work, only in reference [7] there are some experiments for a real moth (Manduca sexta). In reference [8] for a butterfly whose abdomen creates a control moment there are some theories and control design using sliding mode method but no implementation is presented. In reference [5] there are valuable theoretical work and linear controller design for the hover of a flapping wing MAV without the abdomen but unfortunately there is no implementation. DelFlyII MAV has one rotational degree of freedom to produce thrust [6, 9]. The advantage of DelFlyII in producing lift is that it uses a rotation of just one motor and in our paper we used this scheme.
In general, forces and moments created by rudder and elevator are not enough to compensate for atmospheric disturbances. Performance of rudder and elevator depends on the input airflow therefore when decreasing the altitude in hover the role of rudder and elevator can be reversed[10]. This subject makes the autopilot control loops need more sensors and can generate uncontrollable flight situations. Therefore deleting rudder and elevator in a flapping wing MAV's is a good point [10]. Since the abdomen is relatively large, it slows down the dynamics and decreases maneuverability. This type of abdomen can be sensitive to aerodynamic disturbances and creates problems in flight.

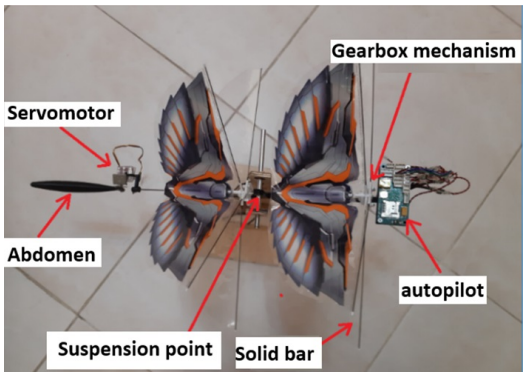

Figure 1: The proposed dragonfly-like MAV with a new structure.

After reviewing the MAV's studies, we see the modeling and simulation of a dragonfly with an active rigid ab-

domen is important and fills the gap. In this paper a new structure consisting of two pairs of mechanisms used in DelFlyII with separated motors for front and back wings like a dragonfly and a rigid abdomen mechanism which can rotate are used as shown in Figure 1.

2 Modelling the multibody dynamics

In this section using Kane's method [11, 12, 13] , the multi-body modelling for the motion of a dragonfly-like MAV will be performed. Dragonfly-like MAV has different parts, a moving rigid abdomen, and a thorax. The kinematics of thorax and abdomen(velocities, accelerations, and angular velocities) will be derived in the inertial frame. Then after calculating external and inertial forces, equations of motion for longitudinal mode will be derived.

2.1 Introducing the structure for the dragonfly-like MAV

In this paper, we used the DelFlyII idea, flapping-wing which is of the type of clap and fling mechanism according to figure 2 is utilized. The recommended structure consists of two pairs of flapping-wing MAV which has eight wings as shown in figure 2. Each flapping-wing separately acts using the change in motor rpm to create lift. Thus, the deferential lift between front and back generates a pitching moment. Each wing from the root of the wing and the leading edge is fixed to fiber carbon bars and the trailing edge of each wing is free with no support. In some plans two more rigid bars are used in each wing. When wings 1 and 2 get close to each other the rigid bars in the leading edges would reach together fast and the trailing edges would reach together slowly. In this situation, the front of wings 1 and 2 are closed and the air is trapped within two wings and it has no way other than leaving from the back and in this way a thrust is produced. This complex motion of wings is done using a motor and a four-link mechanism for wings 1 and 2 and separately for wings 3 and 4.
Another difference between DelFlyII FW-MAV and our FW-MAV is that DelFly has rudder and elevator and it utilizes the flapping mechanism just to produce thrust. As we see from figure 1, the active rigid abdomen with one degree of freedom has just a dynamic role through control moment and despite DelFlyII MAV does not have any rudder nor elevator. Also, the gearbox for this MAV is shown in figure 3.

We have shown wing gearbox mechanism in figure 3. The bars OA, AB, and CB with fixed supports of O and C make a four-link mechanism. In section 3, we will analyze and simulate the gearbox.

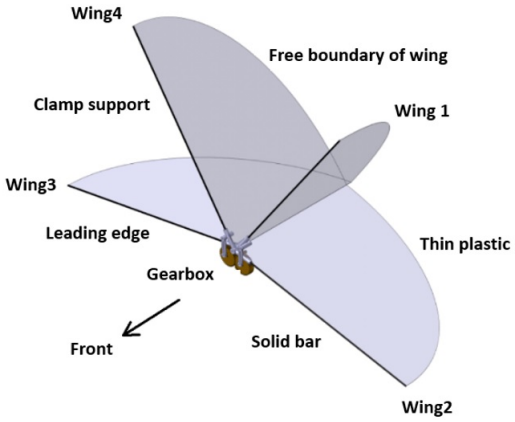

Figure 2: Clap and fling section for DelFlyII MAV.

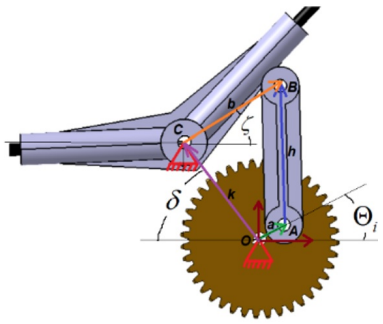

Figure 3: The gearbox and the four-link mechanism.

2.2 Free body diagram kinematics for dragonfly-like MAV

In figure 4, the free body diagram for dragonfly-like MAV is shown. In figure 4, the unit vectors $(\hat{n}_1, \hat{n}_2, \hat{n}_3)$ of inertial frame, $(\hat{b}_1, \hat{b}_2, \hat{b}_3)$ of the frame to fixed dragonfly thorax, and $(\hat{t}_1, \hat{t}_2, \hat{t}_3)$ of the frame fixed to abdomen are defined. There is a one degree of freedom hinge between the abdomen and the thorax. The distance between center of gravity of thorax and H hinge l_t and the distance between hinge is H and center of gravity of abdomen is l_a.
To derive the equations, we ignore the head mass, wing mass, and wing moment of inertia of the MAV. The dragonfly MAV in longitudinal mode has four degrees of freedom, two degrees of freedom for translation, one for rotation of thorax and one for abdomen angle Θ_a. In reference [13] , we have detailed the derivation of equations of motion.
In figure 5, the drag force is denoted by D Also the lift force, velocity vector, angle of attack, pitch angle are indicated by L, V, and α, Θ respectively.

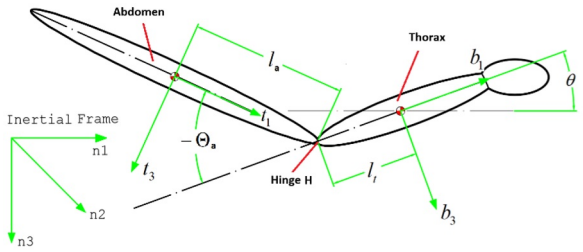

Figure 4: The thorax, abdomen, and inertial frames for dragonfly-like MAV.

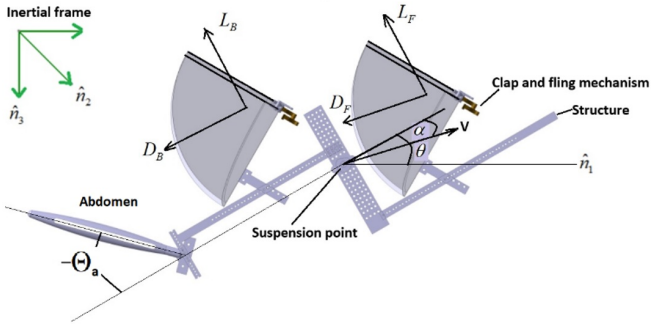

Figure 5: The dragonfly-like MAV at hover (hardware in the loop).

2.3 Longitudinal mode equations using Kane's method

According to Kane's method by after some lengthy algebraic manipulation, the longitudinal mode equations of motion can be derived as the following[19]:

$$
\begin{bmatrix} m_{11} & m_{12} & m_{13} \\ m_{21} & m_{22} & m_{23} \\ m_{31} & m_{32} & m_{33} \end{bmatrix} \begin{bmatrix} \dot{U} \\ \dot{W} \\ \dot{Q} \end{bmatrix} + \\
+ \begin{bmatrix} -(m_a+m_t)QW - m_a l_t Q^2 ... \\ -m_a l_a \cos\Theta_a (Q+Q_a)^2 ... \\ -m_a l_a \sin\Theta_a \dot{Q}_a \\ (m_a+m_t)QU ... \\ +m_a l_a \sin\Theta_a (Q+Q_a)^2 ... \\ -m_a l_a \cos\Theta_a \dot{Q}_a \\ m_a QU(l_t + l_a\cos\Theta_a) ... \\ -m_a l_a l_t \sin\Theta_a Q_a (Q_a+2Q) ... \\ -m_a l_a \sin\Theta_a QW ... \\ +(-I_{ayy} - m_a(l_a^2 + l_a l_t \cos\Theta_a) - m_a l_a^2)\dot{Q}_a ... \\ +C_{mq}Q \end{bmatrix} \\
+ \begin{bmatrix} -(m_t+m_a)g\sin\theta \\ (m_t+m_a)g\cos\theta \\ m_a g l_t \cos\theta + m_a g l_a \cos(\theta+\Theta_a) \end{bmatrix} \\
+ \begin{bmatrix} -D_F - D_B \\ -L_F - L_B \\ L_F b_{FW} - L_B b_{BW} \end{bmatrix} = 0 \tag{1}
$$

In equation (1), values used for m_{ij} of inertial matrix are as follows:

$$
\begin{aligned}
m_{11} &= m_{22} = -(m_a + m_t) \\
m_{12} &= m_{21} = 0 \\
m_{13} &= m_{31} = -m_a l_a \sin\Theta_T \\
m_{23} &= m_{32} = -m_a(l_t + l_a\cos\Theta_a) \\
m_{33} &= -I_{ayy} - I_{tyy} - m_t(l_t^2 + 2l_a^2 + 2l_a l_t \cos\Theta_a)
\end{aligned} \tag{2}
$$

In equation(1), the parameter D_F is front wing drag force, D_B is back wing drag force, L_F is front wing lift force, L_B is back wing lift force, and Q_a is the angular velocity of the abdomen which is produced using a servo. The above lift and drag forces are shown in figure 5. b_{FW} is lift moment arm and is equal to distance between the lift force effective point of front wing and the suspension point for the MAV (cg of the whole MAV is suspended on the base). Similarly b_{BW} is the distance between the effective lift force point for back wing and the suspension point of the MAV. Therefore $\mathrm{L}_F\mathrm{b}_{FW}$ and $\mathrm{L}_B\mathrm{b}_{BW}$ are moments produced from back and front wings lift forces. The difference between these values $\mathrm{L}_F\mathrm{b}_{FW} - \mathrm{L}_B\mathrm{b}_{BW}$ is a differential thrust which creates a pitch moment. Equation (1) is a nonlinear equation for longitudinal mode for the dragonfly-like MAV. The first matrix in that equation is the inertia and the second one matrix in equation 5 consists of non-gravitational forces and the third one matrix consists of gravitational forces. The fourth matrix consists of external forces. L_F and L_B are lift forces for front and back wings, respectively. D_F and D_B are drag forces for front and back wings, respectively.

3 Simulating dragonfly flapping-wing gearbox

In this section first we repeat simulation for DELFLYII MAV gearbox and using the dynamic constraints, we will get a relationship for wing angle and its derivatives with respect to the motor rpm. The basis for the DELFLYII gearbox is a four-link mechanism shown in figure 3. By using kinematic relationship for links, we can derive the following relationship for the gearbox:

$$\begin{aligned}\dot{\zeta} = \dot{\Theta}_i(a/b)(&\cos\Theta_i(k\cos\delta - a\sin\Theta_i + b\sin\zeta)\\ &+\sin\Theta_i(a\cos\Theta_i + k\sin\delta - b\cos\zeta))\\ &/(\cos\zeta(k\cos\delta - a\sin\Theta_i + b\sin\zeta)\\ &+\sin\zeta(a\cos\Theta_i + k\sin\delta - b\cos\zeta))\end{aligned} \tag{3}$$

Equation (3) gives the angular velocity of the wing as a function of mechanism parameters and motor rpm. After simulating this gearbox in MATLAB/Simulink the angular velocity of wing as output with respect to time is plotted in figure 6. By using equation (3) and integrating and differentiating in Simulink, we can get the parameters ζ, $\dot{\zeta}$,$\ddot{\zeta}$. These parameters are needed to calculate the drag and lift forces in section 4.

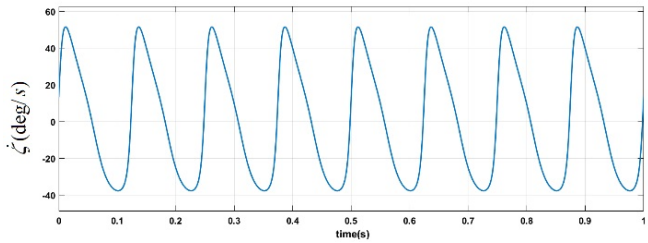

Figure 6: Simulation for flapping-wing gearbox mechanism.

4 Aerodynamic forces calculation (lift and drag)

In reference [6] for an element of the wing, lift and drag forces in body frame are calculated and then using integration in the total area of the wing, a resultant lift and drag forces at each instant are calculated in MATLAB. The resultant quasi-steady aerodynamic forces for a wing rectangular element from the leading edge up to trailing edge in reference [6] is obtained as:

$$d\vec{F} = d\vec{F}_{inertial} + d\vec{F}_{circ} + d\vec{F}_{addmass} - d\vec{F}_{visc} \tag{4}$$

The first portion, inertial forces, is a function of wing mass, fluid mass, wing velocity in z and x directions and the angular velocity of wing around the rigid support at the leading edge. We should mention that side forces in this paper are neglected, i.e. in y-direction we have no force, no acceleration, and no velocity or they do not have any effect on lift and drag. The second portion is circular forces $d\vec{F}_{circ}$, in the third portion we have general forces like $d\vec{F}_{added\,mass}$. Air flow between two wings is not uniform and its velocity changes from a maximum to zero while entering. Therefore, added air between two wings has acceleration and it exerts a force to the wings. It has been explained in reference [6]. The fourth portion is the viscous force which depends on the airflow viscosity that creates a drag force. The obtained forces in equation (4) are forces exerted on a rectangular element of the wing in body frame. To calculate the applied forces on the whole wing, we should integrate forces for this rectangular element in MATLAB software.
In this way the total lift and drag forces in body frame are calculated. After simulating all the aerodynamic relationships reference [6] in Simulink for a motor rpm of 8Hz, it gives the lift and drag for two work cycles in Figures 7 and 8, respectively.

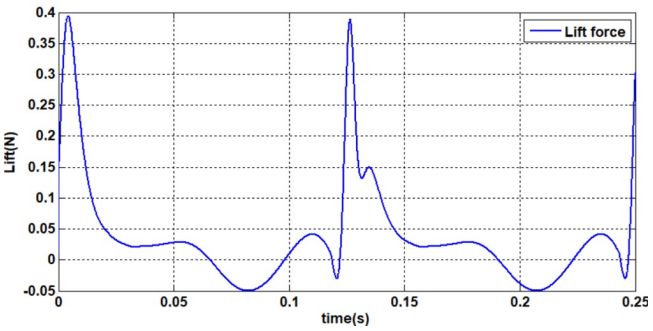

Figure 7: Lift force for rpm of the motor at 8Hz and pitch angle of 80° .

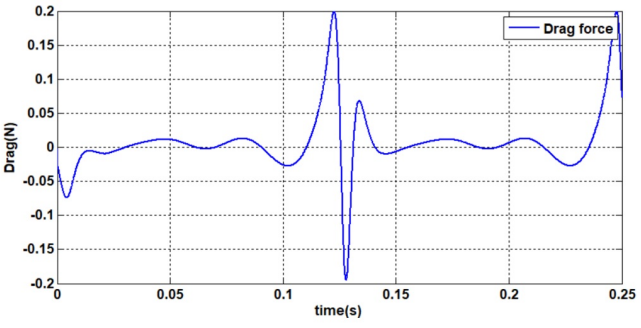

Figure 8: Drag force for the motor rpm at 8Hz and pitch angle of 80° .

As seen from the lift curve in part of a cycle the lift force is even negative but the average lift force in one cycle is positive. Similarly, for drag curve we see that in some portion of a cycle the drag force is even positive but the average drag in one cycle is negative; therefore, positive thrust is created.

5 Linearization around hover point for longitudinal mode on a suspension base

In this section, we want to derive the equations for the MAV pitch angle with one rotational degree of freedom on the suspension base and then by linearizing, we will get the linear equations. Since the base is fixed, we can ignore U and W components of the velocity and put zero for U and W. Thus, adding the aerodynamic moment from C_{mq} and doing some algebraic manipulation in equation(1), we will get the following equation:

$$\begin{aligned}&(-I_{ayy}-I_{tyy}-m_a(l_t^2+l_a^2+2l_al_t\cos\Theta_a))\dot{Q}=\\&\ m_al_al_t\sin\Theta_aQ_a(Q_a+2Q)-m_agl_t\cos\theta\\&-m_agl_a\cos(\theta+\Theta_a)\\&-(-I_{ayy}-m_a(l_a^2+l_al_t\cos\Theta_a))\dot{Q}_a\\&+C_{mq}Q-b_{FW}\times L_F+b_{BW}\times L_B\end{aligned}\tag{5}$$

In equation (5), L_F is lift force for front wings, L_B is lift force for back wings,b_{FW} , b_{BW} are the distance between the effective point of lift of front (back) wings and the suspension point. The suspension point is assumed to be located on the CG of the MAV.
Assuming the state variables $x_1=\theta$ and $x_2=\dot{\theta}$, equation (5) after some algebraic manipulation can be written as follows:

$$\begin{cases}\dot{x}_1=x_2\\ \dot{x}_2=(m_al_al_t\sin\Theta_aQ_a(Q_a+2x_2)...\\ \quad -(-I_{ayy}-m_a(l_a^2+l_al_t\cos\Theta_a))\dot{Q}_a...\\ \quad -m_agl_t\cos x_1\ -m_agl_a\cos(x_1+\Theta_a)...\\ \quad -L_F\times b_{FW}+L_B\times b_{BW})+C_{mq}x_2...\\ \quad /(-I_{ayy}-I_{tyy}-m_a(l_t^2+l_a^2+2l_al_t\cos\Theta_a))\end{cases}\tag{6}$$

The aim of this portion is to linearize equation (6) around the hover point (the hover is defined as the point which the MAV can suspend itself on the desirable pitch angle which is assumed to be 80° in this paper). The main challenge to linearize is due to not having an explicit relationship between lift force and the longitudinal angles and actuator input (the system consisting of motor and the gearbox which rotates the wings). For linearization, we should differentiate the lift force with respect to θ and $\dot{\theta}$ shown in section 4. On the other hand, ζ in equation (3) and its derivatives in the gearbox simulation equation are nonlinear. These two issues make calculation of Jacobian for linearization impossible. Therefore, we cannot derive an explicit linear relationship for any desirable angle of hover. As an example, we linearize the system around a hover angle of 80°.
To resolve the linearization challenge, we used simulation for aerodynamics in Simulink twice around 80° (with ±5°). According to figure 9, we see that for ±5° deviation of hover, the average lift in each flapping cycle changes less than one percent, therefore we can ignore the lift derivative with respect to angle θ of the MAV. Thus, we can have:

$$\partial L_B/\partial x_2=\partial L_F/\partial x_2=\partial L_B/\partial x_1=\partial L_F/\partial x_1\simeq 0\tag{7}$$

Another problem in linearization is calculating the lift and drag force derivatives with respect to gearbox motor rpm. To resolve this problem, we used the theorem of average function for each flapping cycle. To do this, a program in MATLAB is written which changes the motor rpm from 1Hz to 15Hz with a step of 0.1 for lift and drag simulation. A second-degree curve was fitted to the results. Then using the interpolation, the results are shown in figure 10.
By interpolation, the average lift force function with respect to rotational frequency of the motor can be derived as follows (150 times aerodynamic simulations for different rpm of the motor were run):

$$L=0.0008f_{motor}^2-0.0025f_{motor}\tag{8}$$

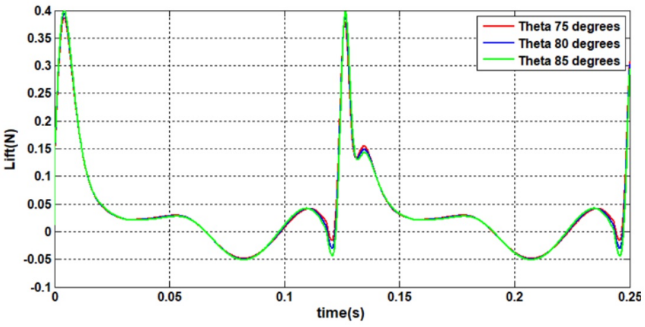

Figure 9: Change of lift force in two cycles for different pitch angles .

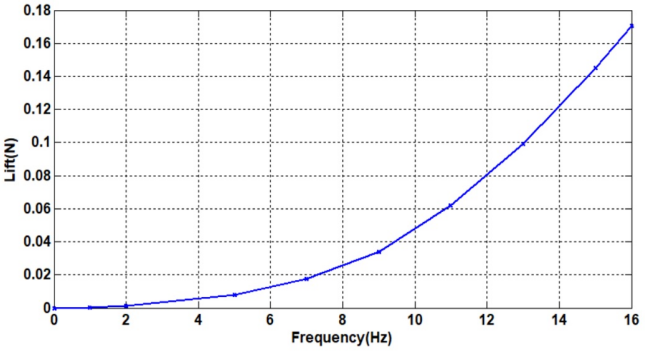

Figure 10: Lift force with respect to motor rpm of flapping-wing MAV .

Therefore, the challenge of the differentiating lift with respect to rpm of the motors for linearizion will

be eliminated by using equation (8). In equation (6), by equating zero, the trim point will be obtained:

$$\begin{aligned} x_1 &= \pi/2 \\ x_2 &= 0 \end{aligned} \tag{9}$$

The physical concept for this equilibrium position for the MAV with abdomen which was a two-body system was similar to the equilibrium of a double pendulum. But if we want to hover around 80°, we should assume the equilibrium as 80° and we should transfer the state space equations to this point. The general form of the state space is as follows:

$$\dot{x} = Ax + Bu \tag{10}$$

After transferring to the trim point of 80°, we can write the state equations as follows:

$$\dot{x} = A \begin{bmatrix} x_1 - \frac{80\pi}{180} \\ x_2 \end{bmatrix} + Bu \tag{11}$$

In equation (11), $u = [\dot{Q}_a \, \Delta L \, \Theta_a]$ is the input vector which includes $\dot{Q}_a$ that is the angular acceleration applied to the abdomen of the MAV through the servomotor and creates the control moment and $\Delta L = L_B - L_F$ creates the differential lift.
We have assumed the trim state (equilibrium) is the state in which the MAV has a pitch angle of 80° and the abdomen is along the thorax ($Q_a = -\Theta_a = 0$). The numerical values of matrices A and B based on the geometrical and inertia /mass specifications and equilibrium state values in Jacobian can be obtained as follows (according to values in Table 1 for the designed MAV):

$$A = \begin{bmatrix} 0 & 1 \\ -19.88138 & 0 \end{bmatrix} \tag{12}$$

$$B = \begin{bmatrix} 0 & 0 & 0 \\ -0.126106 & -38.28667 & -5.0859346 \end{bmatrix} \tag{13}$$

According to equation (11), we see the linearized equations for the MAV with an active rigid abdomen and clap and fling mechanism for hovering around 80° on the suspension base were obtained:

$$\begin{aligned} \dot{x} = &\begin{bmatrix} 0 & 1 \\ -19.88138 & 0 \end{bmatrix} \begin{bmatrix} x_1 - \frac{80\pi}{180} \\ x_2 \end{bmatrix} \\ &+ \begin{bmatrix} 0 & 0 & 0 \\ -0.126106 & -38.28667 & -5.0859346 \end{bmatrix} \begin{bmatrix} \dot{Q}_a \\ \Delta L \\ \Theta_a \end{bmatrix} \end{aligned} \tag{14}$$

To verify the linearization, the simulation response for linear and nonlinear models are compared in figures 11 and 12. For the MAV to be stable at angle of 80°, there should be a moment which is from the difference in motor rpm which results in differential thrust at each flapping cycle. By doing some simulations, this value would be -0.0037 (the minus sign is for the direction of the moment). As a physical explanation, to stabilize the open-loop, the force from the back wings should be more than that of the front wings. It creates the differential moment and that would result in the MAV to be fixed at 80° (otherwise the MAV would go in the vertical direction). By using this value for the moment, differential lift force can be obtained from equation (15):

$$L_B - L_F = \frac{0.0037}{0.04} = 0.0925N \tag{15}$$

Assume that we want the rpm of the back wings to be 15Hz, this motor rpm based on the simulation results using equation (14) would mean that the average lift force in each flapping cycle would be equal to $L_B = 0.1425N$. Therefore, according to equation (8), the average lift force for the front wings in each flapping cycle would be equal to 0.05N. We can assumed that the MAV is on the suspension base and the summation of the lift force of front wings and back wings would be less than or equal to total weight:

$$L_F = 0.05N \tag{16}$$

This average value for wing lift force based on simulation results or equation (14) would happen at motor rpm for front wings with a frequency of 9.4Hz. These two motor rpm would create a hover of 80 degrees in the open-loop case.

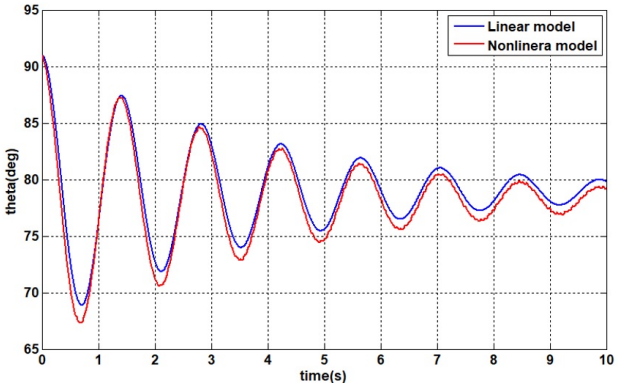

Figure 11: The comparison of body pitch angle in linear and nonlinear cases .

In summary, the control input was obtained for equilibrium conditions for the MAV at hover with an rpm frequency of front motor rpm at 9.4Hz and back motor rpm at 15Hz and an angle of attack of 25° and a pitch angle of 80°. We should mention that in simulation, we have added C_{mq} damping to the simulated equations similar

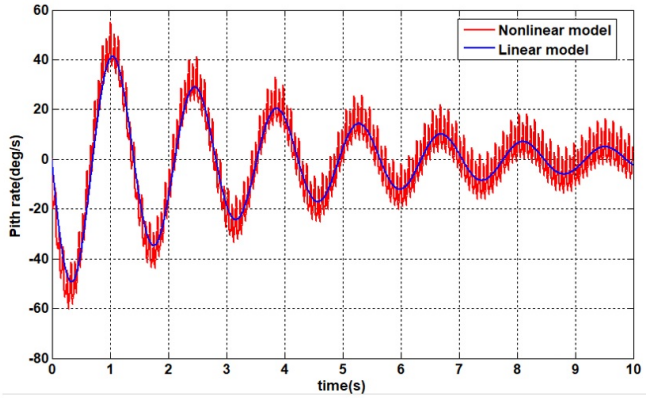

Figure 12: The pitch rate of the body in linear and nonlinear case .

to the case in real flight. The air viscosity would damp oscillation of pitch angle, the effect of C_{mq} damping can be seen in figures 11 and 12 time responses. We have assumed the initial conditions for pitch angle at $\theta_0 = 91°$ in linear and nonlinear simulations.
As we see in figure11, the pitch angle of the MAV would oscillate around 80°. In figure 12 we see the pitch rate as the output of the simulation for the MAV and we see that a frequency based on flapping would ride on nonlinear response. As we see the nonlinear and the linear responses are close to each other and in this way the linearization process and the assumptions made to resolve the challenges are verified.

6 Designing and manufacturing the dragonfly-like MAV and introducing its hardware

The values of parameters of the dragonfly like MAV and the specifications of the system are shown in Table 1.

In figure 13 the dragonfly like MAV is shown at hover position at an angle of 80°.

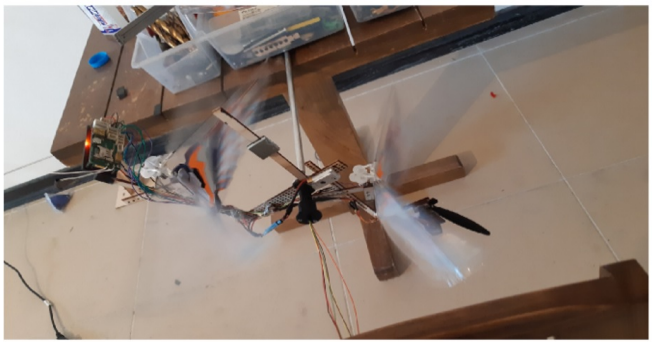

Figure 13: The dragonfly-like MAV at hover (hardware in the loop).

a	0.0045	m
b	0.00647	m
b_{BW}	0.04	m
b_{FW}	0.04	m
d	0	m
h	0.0215	m
I_{tyy}	0.000569	$kg.m^2$
I_{ayy}	1.35e-5	$kg.m^2$
l_t	0.16	m
l_a	0.055	m
M_{wing}	0.00029	kg
m_t	0.11	kg
m_a	0.01	kg
R_w	0.0137	m

Table 1: parameters of the dragonfly like MAV used in simulation.

To implement the controller, we need some elements like micro brush motor, the speed controller board for micro brush motor, Apogee autopilot board, Paparazzi software, DELFLY gearbox system and the wings, a servo motor, lithium battery and slip ring, and the USB serial converter. These hardware elements are shown in figure 14.

7 Implementing hardware in the loop controller by using Paparazzi Apogee board V1

In previous sections of this paper, the equations of dragonfly like MAV were simulated in Simulink MATLAB. In this section, the Simulink file was created such that we can relate the Simulink with Paparazzi software real time and we can send the control commands to Apogee board hardware and get sensors feedback. Implementing the control algorithm on a software consists of two main sections:
I- software and hardware of autopilot
II- Simulink software and its interface with autopilot
In this section first we explain the needed hardware to control the MAV. To control the actuators of the MAV (two micro brush motors for back wings and front wings and servomotor for moving the abdomen), which are of DC motor type, we use a hardware named ESC or electronic speed controller. This hardware consists of voltage and PWM signal as inputs and voltage to the DC motor as the output. The width of the input PWM signal to hardware can be changed from 1000ms to 2000ms which and it correspond to zero speed and the maximum speed of the motor, respectively. This hardware while connected to the autopilot would receive desired motor speed in the form of PWM signal and would apply to the motor instantaneously. In other words, the interface between DC motors and autopilot is the ESC

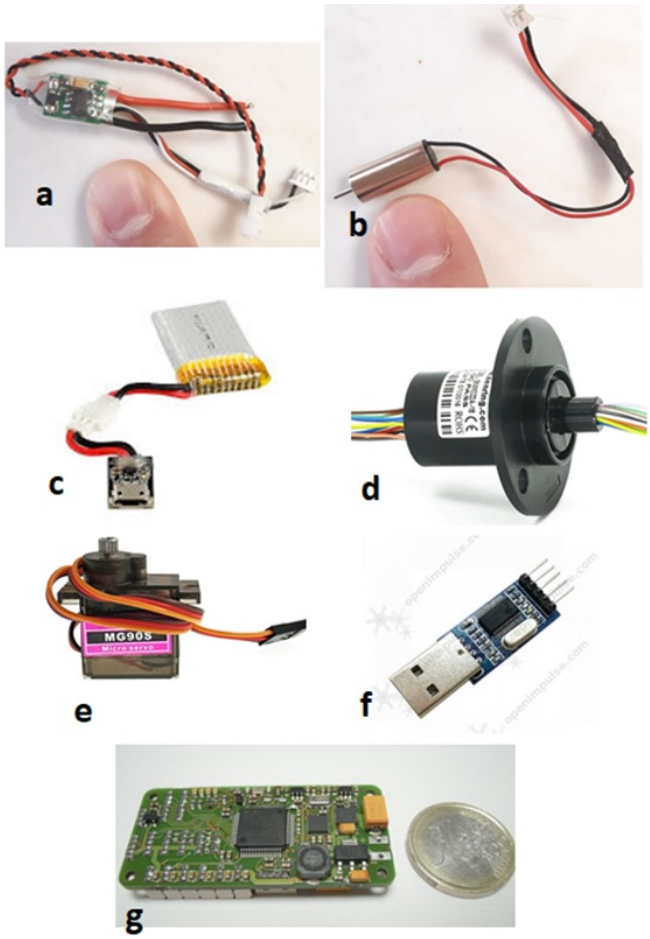

Figure 14: The important portions of hardware: a- speed control micro brush motor b- micro brush motor, c- battery d- slip ring, e- servo motor f- serial to USB converter, g- Apogee autopilot board version 1 .

hardware.

8 Designing and implementing an LQR controller

In designing an LQR control, the criteria for the performance of the system is introduced with a cost function of J, in which the controller tries to minimize it. This cost function is calculated as follows:

$$J = \int_0^\infty [x^T Q x + u^T R u] dt \tag{17}$$

In which Q is a positive semidefinite weighting matrix and can be normalized using the maximum values for states. The control weighting matrix R is a positive definite. Based on the actuator physics we should choose a suitable value for it. The R and Q matrices are very important regarding the errors. To have a successful LQR design, these matrices should be chosen very carefully. In this paper we use Bryson's rule. According to Bryson's rule, Q and R matrices are diagonal ones having elements on the main diagonal as inverse of the square of maximum values for states and control, respectively. The coefficient of the expression for $\dot{Q}_a$ in the equation of motion has the units as moment of inertia and therefore the expression $(-I_{ayy} - m_a(l_a^2 + l_a l_t \cos\Theta_a))\dot{Q}_a$ is equivalent to the moment that is exerted on the abdomen. We used $\dot{Q}_a$ as control input. The maximum values for pitch angle and pitch rate based on motor rpm and open-loop simulation results are determined as follows:

$$\begin{aligned} |\theta| &= |x_1| \leq 5^\circ \\ \left|\dot{\theta}\right| &= |x_2| \leq 20^\circ/\sec \end{aligned} \tag{18}$$

Based on the above values, Q can be determined as follows:

$$Q = \begin{bmatrix} \frac{1}{(5\pi/180)^2} & 0 \\ 0 & \frac{1}{(20\pi/180)^2} \end{bmatrix} \tag{19}$$

The control input is the product of lift force and the distance between suspension point to the effective point of lift force. Therefore, its maximum is proportional to maximum lift and can be obtained from equation (20):

$$-(-I_{ayy} - m_a(l_a^2 + l_a l_t \cos\Theta_a))\dot{Q}_a \leq -b_{FW} \times L_F + b_{BW} \times L_B \tag{20}$$

After substituting the values, maximum $\dot{Q}_a$ can be obtained from equation (21):

$$\dot{Q}_a \leq 6.072 \tag{21}$$

In the hardware in the loop, we fixed the abdomen and did not use $\dot{Q}_a$ as input. Therefore, the R matrix based on the maximum values for inputs can be obtained from equation (22):

$$R = \left[\frac{1}{(\Delta L_{\max})^2}\right] = \left[\frac{1}{(0.02 \times 9.81)^2}\right] \tag{22}$$

Now having matrices A, B, Q, and R, we can write Riccati equation as follows:

$$A^T P + PA - PBR^{-1}B^T P + Q = 0 \tag{23}$$

We can obtain matrix P from the Riccati equation and then calculate optimal control gain (K) as in equation (24):

$$K = R^{-1}B^T P \tag{24}$$

After substituting the values for the gain matrix can be obtained as follows:

$$K = \begin{bmatrix} -2.0433 & -0.6586 \end{bmatrix} \tag{25}$$

The above controller gains were applied on linear model as well as to the nonlinear model and we can compare the responses.

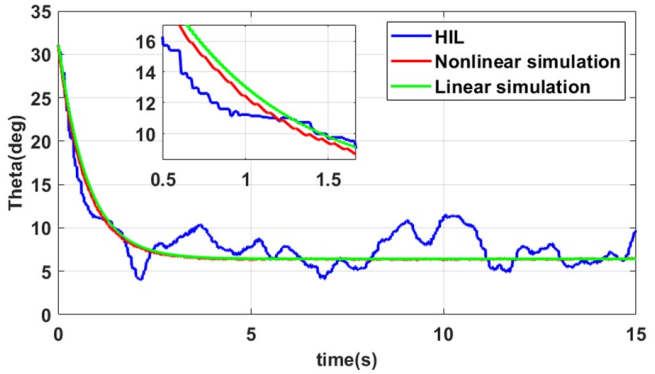

Figure 15: The closed loop time responses of for linear and nonlinear models.

The MAV is released from $\theta = 31°$ considering the equilibrium point of $\theta = 5°$. The time responses for the closed loop for θ are obtained as in figure 15 for linear and nonlinear models. By comparing the linear and nonlinear responses, it is observed that LQR gain which was obtained for linear model can work for nonlinear model as well.

9 Conclusions

In this paper, a new structure for the dragonfly-like MAV which had flapping wing with active rigid abdomen was proposed. Unlike previous research works, the abdomen of this MAV has no control role in flight. The nonlinear equations of motion were presented for two-body system in the presence of aerodynamic forces and the gearbox for the dragonfly-like MAV with active rigid abdomen. Then, the nonlinear dynamic equations of motion with nonlinear aerodynamics and nonlinear gearbox relationships were linearized. The good agreement between linear and nonlinear responses confirmed the validity of linearized equations. The positive role of abdomen motion in the open-loop as a vibration damper to create the left half-plane poles were discussed and analyzed. The LQR controller was designed for the linear system and the obtained gain was applied to both the linear and the nonlinear models. The closed loop responses were then compared. Moreover, hardware in the loop tests were performed using Paparazzi software and Apogee autopilot board. The results demonstrated appropriate robustness and accuracy of the designed controller as well as good agreement with numerical simulations in the presence of disturbances during real flight. In future works, the six degrees of freedom equations of motion similar to the longitudinal mode would be obtained. Furthermore, the controller design would be accomplished for the 6DOF case to study the abdomen role in stability.

References

[1] Anders Hedenström. Extreme endurance migration: what is the limit to non-stop flight? PLoS biology, 8(5):e1000362, 2010.

[2] Kimon P Valavanis. Advances in unmanned aerial vehicles: state of the art and the road to autonomy. 2008.

[3] Gareth D Padfield. Helicopter flight dynamics: including a treatment of tiltrotor aircraft. John Wiley & Sons, 2018.

[4] Hao Jie Zhu, Xue Guang Meng, and Mao Sun. Forward flight stability in a drone-fly. Scientific reports, 10(1):1–12, 2020.

[5] Shiba Biswal, Marc Mignolet, and Armando A Rodriguez. Modeling and control of flapping wing micro aerial vehicles. Bioinspiration & biomimetics, 14(2):026004, 2019.

[6] Sophie F Armanini, JV Caetano, GCHE De Croon, CC De Visser, and Max Mulder. Quasi-steady aerodynamic model of clap-and-fling flapping mav and validation using free-flight data. Bioinspiration & biomimetics, 11(4):046002, 2016.

[7] Jonathan P Dyhr, Kristi A Morgansen, Thomas L Daniel, and Noah J Cowan. Flexible strategies for flight control: an active role for the abdomen. Journal of Experimental Biology, 216(9):1523–1536, 2013.

[8] Jeeva Jayakumar, Kei Senda, and Naoto Yokoyama. Control of pitch attitude by abdomen during forward flight of two-dimensional butterfly. Journal of Aircraft, 55(6):2327–2337, 2018.

[9] Joao V Caetano, CC De Visser, GCHE De Croon, B Remes, C De Wagter, J Verboom, and M Mulder. Linear aerodynamic model identification of a flapping wing mav based on flight test data. International Journal of Micro Air Vehicles, 5(4):273–286, 2013.

[10] Christophe De Wagter, Matěj Karásek, and Guido de Croon. Quad-thopter: tailless flapping wing robot with four pairs of wings. International Journal of Micro Air Vehicles, 10(3):244–253, 2018.

[11] Michael Bolender. Rigid multi-body equations-of-motion for flapping wing mavs using kane's equations. In AIAA Guidance, Navigation, and Control Conference, page 6158, 2009.

[12] Thomas R Kane and David A Levinson. Dynamics, theory and applications. McGraw Hill, 1985.

[13] Mohammad Lashgari and Abolghasem Naghash. Modeling and linearization of longitudinal dynamics for a flapping wing micro aerial vehicle dragonfly-like with active rigid tail. Amirkabir Journal of Mechanical Engineering, 53(6):2–2, 2021.

10 nomenclature

a, b	link length of the mechanism
b_{BW} , b_{FW}	Distance between the effective lift force point for the back(front) wing and the suspension point
C_{mq}	pitching moment coefficient
D_F , D_B	Front(back) wing drag force
f_{motor}	MAV gearbox motor frequency
$F_{addedmass}$	Added mass forces
F_{circ}	Circulatory forces
$F_{inertial}$	Inertial forces
F_{visc}	Viscous forces
g	gravitational acceleration
h	second link length of the mechanism
I_{tyy} I_{ayy}	Thorax (abdomen) moment of inertia
L	Lift force
L_B L_F	The Back(Front) wing lift force
l_t l_a	Distance between CG of the thorax(abdomen) and the hinge
m_t m_a	Thorax(abdomen) mass
Q	Thorax pitch rate, the weighting matrix
Q_a	Abdomen angular velocity relative to thorax
$\dot{Q}_a$	Abdomen angular acceleration relative to thorax
R	control weighting matrix
U	MAV velocity component in x-direction of the body frame
u	Input control vector
W	MAV velocity component in z-direction of the body frame
α	Angle of attack
δ	Fixed angle of gearbox
ΔL	Differential lift
θ	Pitch angle
θ_i	Input angle of the gearbox
θ_a	Abdomen angle
ζ	Wing flap angle

Table 2: parameters of the dragonfly like MAV used in simulation.